Liquid Crystal Based 5 cm Adaptive Focus Lens to Solve Accommodation-Convergence (AC) Mismatch Issue of AR/VR/3D Displays

Amit K Bhowmick*, Afsoon Jamali**, Douglas Bryant*, Sandro Pintz**, Philip J Bos*

***Advanced Materials and Liquid Crystal Institute, Kent State University, Kent, OH**

****Facebook Reality Labs, Redmond, WA, USA**

Abstract

Vision discomfort due to the accommodation-convergence mismatch remains a challenge for current HMDs used for VR/AR applications. A potential solution of this issue is to use an adaptive focus lens that is lightweight, flat and has a large aperture. In this paper, we present a 5 cm diameter Liquid Crystal based focus tunable lens. Despite the large aperture, the lens has characteristics of fast switching speed(500ms), low driving voltage (<5 V), and low thickness (<5mm).

Author Keywords

Adaptive Lens, Accommodation-Convergence Mismatch, Liquid Crystal Lens

1. Introduction

Head-mounted displays (HMDs) are on the verge of making a revolution in the field of education, entertainment, and communication. However, there are challenges related to optics yet to be solved. Such near-to-eye displays can provide natural, and comfortable visual experience only if the device system is tailored to mimic complicated image formation mechanism of human eye-brain visual system.

In current HMDs, for the VR application, a physical display is placed behind a fixed magnifying lens. The role of fixed magnifying lens is to create a virtual image at a fixed distance, where human eye tries to accommodate. However, stereographic images on the displays converge to different distances depending on depth of relative objects. To sense stereographic depth of virtual images, human eye changes the vergence angle despite accommodation distance due to fixed magnifying lens remain the same. This conflict is known as accommodation-convergence (AC) mismatch, which results in eyestrain, and unnatural user experience [1]

Shibata et al. have provided a comprehensive review of this problem, where he relates the issue by defining "zone of comfort". The "zone of comfort" is when the mismatch between focus power needed to match the accommodation distance, and the convergence point distance is within 0.5 D [2]. Several approaches have been addressed to solve the issue: light field displays [3, 4], volumetric displays [5], and digital holography displays [6]. In light field display, multiple perspectives of virtual image is projected into different parts of the pupil which creates a field of light what eye would see in real world. However, Takaki and Kikuta showed that eyes will focus correctly if each pixels of the display emit 16 times more rays than conventional 2-D HMDs [7]. Hence, the image resolution is significantly reduced. In volumetric display [5], field sequential volumetric displays continuously render objects of different depth and adjust the apparent display distance. However, reported approach of volumetric display increases bandwidth of the display by two to six times. Digital holography display is another approach, where field of view is increased by magnifying the projector through diverging light [6]. However, for high image quality, an increase in the field of view requires smaller eye-box. Hence, additional optical elements like beam steering devices are required for pupil expansion of such technology.

Recently, Kramida and Varsney did an extensive literature review about the prospect and drawbacks of each proposed solution of AC mismatch issue and concluded that varifocal LC lenses coupled with eye-tracking system have the highest potential for solving the issue [8]. We previously proposed and demonstrated a solution to the AC mismatch problem with an eye-tracked tunable liquid crystal lens [9–11] with an aperture size of 2cm. To provide an optimum field of view (FoV) in VR devices, there is a need for larger aperture size (>2 cm) tunable lenses. However, larger aperture sized adaptive focus lenses are challenging for all available adaptive focus lenses technologies. Stevens et al. conducted extensive literature reviews available tunable lens technologies for HMDs and reported non-mechanical adjustable lenses more than 20 mm in diameter are not reported yet commercially [12]. In this report, we present a 50 mm aperture size LC-based continuous focus lens.

2. Design concept of the proposed device

Although diffraction-limited performance has been reported on 2.4 mm aperture liquid crystal lens, LC-based large aperture lens more than 10 mm has been a challenge for a long time. The optical path difference (OPD) of a liquid crystal lens depends on cell thickness. From the thin lens equation, the OPD of an ideal lens is proportional to the square of the lens radius. This requires that the thickness of the LC cell is also proportional to the square of the lens radius. On the other hand, switching time of an LC cell depends on viscosity of the LC material and cell thickness. For a given LC material, the switching time is proportional to the square of cell thickness. Hence, for LC-based lenses, switching time is proportional to the fourth power of the lens radius.

To keep the switching speed within a reasonable time (< 500 ms) for a 50 mm aperture sized LC lens, we first have considered to have the desired lens to be comprised of two LC cells that are of half the required OPD for the desired optical power. With this approach the viewing angle performance of the lens is also improved, as demonstrated by Li et al. [15].

However, to further enable a large-aperture lens with low switching speed, we have implemented Fresnel resets in the design. In contrast to an ideal lens, the OPD of the designed lens will provide a stepwise increase in optical path length. The introduction of Fresnel resets can cause diffraction and image degradation. However, if the stepwise phase increment is integer multiple of the wavelength of the viewed light, then diffraction-limited performance is expected to be achieved. Worst-case diffraction performance occurs when phase step increment on the reset boundaries is half-integer multiple of wavelength [13, 14]. In such case, the incoming beam splits into two beams. However, if the angle between two split beams is within human eye angular resolution of 1 arc min then a user cannot distinguish the diffracted image. Previously we showed that, within a 20 mm diameter area

around the center of a 0.5D lens, the diffraction from out of phase zone boundaries will be under 1 arc minute. However, outside of this radius the diffraction angle will exceed 1 arc minute. The degree of resulting image degradation is the subject of this paper.

3. Example lens

As an example lens, we are considering a 50 mm aperture sized lens, which can provide a 0.80 D optical swing. The lens is a stack of two liquid crystal cells of opposite rubbing direction. Each cell is capable of continuous change optical power from – 0.20 D to + 0.20 D, in other words, 0.40 D of optical swing of each of the cells. We have used liquid crystal material MLC 18349, which has a birefringence value of 0.27. From thin lens equation (1),

$$OPD_{cell} = \frac{r^2}{2f} \qquad (1)$$

OPD variation for (+/- 0.20 D) optical power lens of 2.5 cm radius is equal to 62 µm or 114 **λ** (designed wavelength, **λ** = 543.5 nm). Relating with OPD equation ($OPD_{cell} = \Delta n \cdot d$) of a liquid crystal cell of thickness d, to achieve 114 **λ** OPD, the required cell gap is 287 µm . (Here, we have assumed that we can use 80% optical swing of LC material.) By considering 28 Fresnel segmented resets on the designed LC lens, we can reduce the thickness of the lens cell to approximately 12 µm**.** Therefore, with the Fresnel resets, the switching time of the lens is increased by 28^2= 784 times. Additionally, the stacking of two cells of +/- 0.20 D further reduces the switching time by $(2)^2$= 4 times. The phase map of a single-lens cell with 28 phase resets is shown in figure 1.

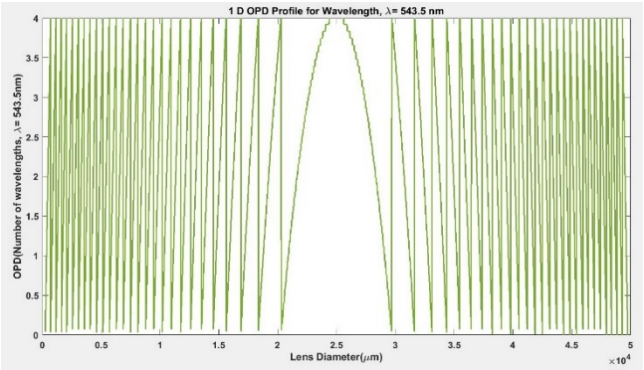

Figure 1. Change of phase (OPD) of 28 Fresnel resets LC lens in terms of number of wavelengths of designed wavelength (λ= 543.5 nm). Each Fresnel reset/zone contributing 4 λ of optical path difference.

In our device, continuous phase change across the lens diameter is controlled through applying electric field on concentric ring electrode structures (Fig. 2). Phase change on ring electrodes is controlled by an applied electric field. As we desire to achieve parabolic phase change across the lens area, the width of each electrode also changes in a parabolic manner, but the area of each ring remain constant. Every ring electrode is internally connected by an inner ring resistive network to provide precise voltage drop across adjacent electrodes.

The change of OPD of liquid crystal material is not linear with applied voltage, (the change of OPD is steeper at lower applied voltage). As a result, only two interconnections do not work for our proposed device. Instead, we have proposed to drive the lens by eight Nickel bus-lines. The region of the cell between two bus-line connections corresponds to a section of the OPD vs. voltage curve

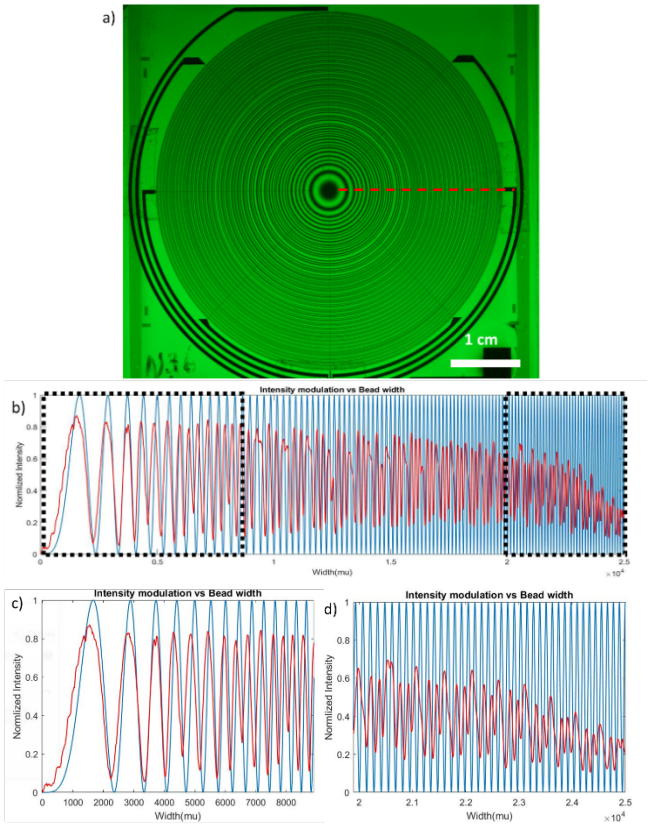

Figure 2. Phase profile of fabricated lens. a) continuous phase variation across 50 mm aperture of lens cell tuned for + 0.20 D, the lens cell is placed at 45 degrees between a cross polarizer and the picture is taken with green (λ = 543 nm) light filter. b) phase variation plot compared to the ideal case along the red dashed lines of (a), red and blue solid lines represent fabricated lens phase and ideal phase, respectively. (c), (d) showing zoomed view of left and right dotted black box of (b)

that is linear. The value of resistors and Via positions are selected in such a way that the voltage profile can be controlled by Nickel bus line connections to get the desire phase profile.

To obtain voltage drop across adjacent electrodes through a resistor network, we must include a gap between adjacent electrodes (Fig. 3(a)). However, relatively weaker electric field in the electrode gap area creates phase bump in that region. Li et al have shown a smaller electrode gap is favorable to avoid phase jump, however, considering shorting issue electrode gap less than 2um is challenging to fabricate [15]. Li el al also showed that a second ITO electrode layer can be deposited on top of first driving ITO electrodes to cover the electrode gap area [16]. In contrast to 1st layer driving electrodes, 2nd layer ITO is capacitively coupled to driven electrodes and were called floating electrodes. In addition to covering electrode gap, floating electrode also increase phase change steps across the electrodes, which helps to improve image quality by reducing background haze. In our proposed device, we have implemented 2 µm electrode gaps between driven electrodes, and floating electrodes are fabricated on top of driven electrodes to cover the inter-electrode gaps (Fig. 3**.** (b)). Change of retardation color within a zone is shown on Fig. 4.

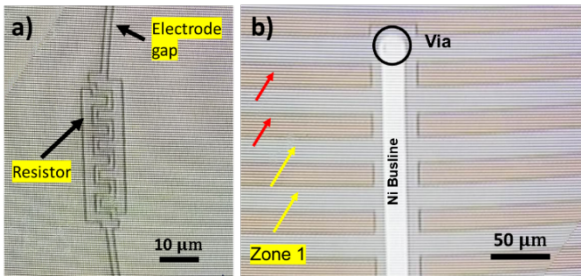

Figure 3. a) Showing resistor and electrode gap between two driven electrodes, (b) yellow, red mark shows floating electrodes and exposed part of driven electrodes, respectively; black circle shows location of Via connection on Ni bus line The photo is taken in the middle of fabrication process, the floating electrodes contain photoresist on top, as a result, more reflective than exposed driven electrodes.

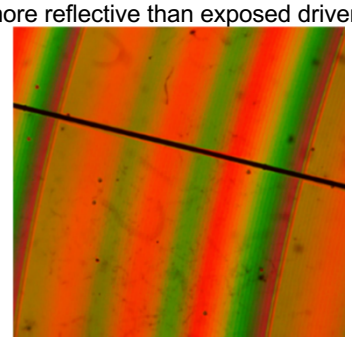

Figure 4. Change of phase retardation across zone 3.

4. Fabrication

To fabricate a test 2.5 cm radius lens, we first pattern-driven electrodes and ground plate electrode of the lens on commercially available ITO coated glass (thickness 0.4 mm). After that we put SiO_2 insulator layer on top of driven ITO and pattern with a via photomask. Next, we etch SiO_2 from via positions with RIE dry etch process. Etching of SiO_2 layer from via locations reveals underneath driven ITO layer. For the next process steps, we deposit Nickel and pattern it to form bus lines, which connect selected ITO electrodes to a bonding pad. To add floating electrodes, an additional layer of an insulator is deposited to protect Ni during the following floating ITO etch process. The thickness of the insulator is preferred to be small to ensure stronger capacitive coupling between floating electrodes and the driven electrode layers. Over the 2nd layer of SiO_2, a very thin layer of ITO is deposited and patterned for the floating electrodes. After the patterning process, the polyimide (SE-2170) layer is spin coated on the patterned bottom and top substrates; rubbed the PI layer in such a way that the rubbing direction is opposite for top and bottom substrates—fig. 5 (a) side view of inner layer structure of the lens. Finally, the cell is assembled and filled following standard LCD fabrication process.

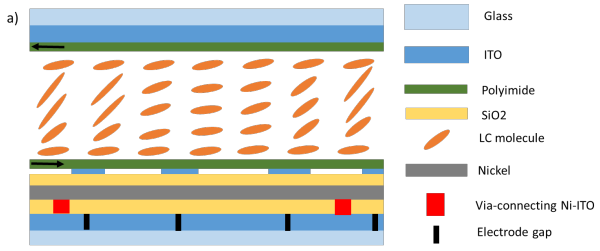

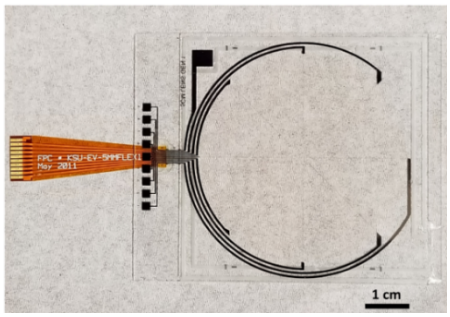

Figure 5. Fabricated lens cell, a) Schematic diagram of the side view of the inner layer structures of the lens, b) fabricated 50 mm aperture LC lens

The Nickel bus line connectors are connected to a flex bonding, where the driving voltage will be applied. Final look of the build cell is shown on Fig. 5 (b)

5. Image Quality Test

Image quality of the fabricated lens is tested using a negative USAF 1951 test target with fluorescent light illumination on the back. A linear polarizer is placed before the lens cell. The polarization direction of the used polarizer is along the rubbing direction of the cell. Pictures shown in figure 6 is taken using Canon EOS Rebel XSi/450D and 100 mm macro lens. To evaluate image quality of a lens cell for near-to-eye display application, we have used an aperture stop of diameter 5 mm, which was attached to LC lens surface. LC lens with aperture stop is attached to head of Canon camera lens. The aperture stop size was chosen to consider the average diameter of human eye's pupil.

Hence, in our system, on-axis light polarized light passing through the lens and aperture stop, and image is formed on DSLR image sensor. To understand the effect of different zone boundary densities on the image performance, we translate the aperture stop position by 5 mm in consecutive steps from the center of the lens towards the edge. If we consider that center of eye's is 2 cm away from the lens, then the cases shown in Fig. 6. (a), (b), (c), (d), (e), (f) corresponds to 0°, 0°, 14°, 27°, 37°, 45° gaze angles, respectively.

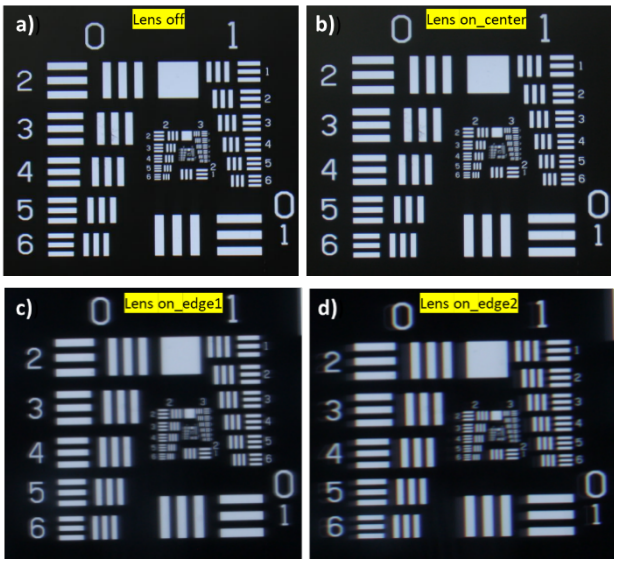

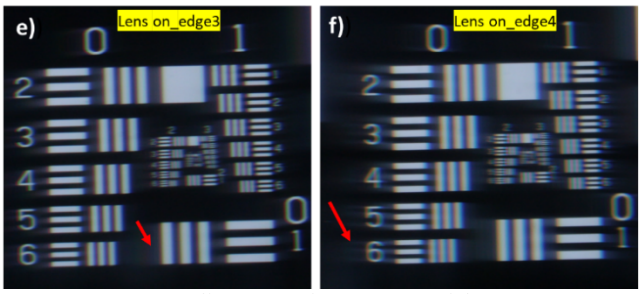

Figure 6. Image quality comparison. Center of the DSLR camera lens is placed at 0 mm away from the center of the lens for (a), and (b); 5 mm, 10 mm, 15 mm, and 20 mm away from the center of the lens for (c), (d), (e), and (f), respectively. On the figure, (a) lens off, and (b), (c), (d), (e), (f) lens on with power + 0.20D. The red arrow shows the diffracted image on the picture.

We have seen diffracted images when the center of the camera lens is shifted closer to the edge of the tunable LC lens, where zone reset density is high (approximately 10 reset zones within aperture stop for Fig. 6 (e)). Calculation shows that the diffracted image distance correlates with average zone widths for each case.

MTF is measured from the green channel contrast ratio of group 1 element 1, which corresponds to spatial frequency 10 Cyc/degree according to our optical setup. MTF value obtained from Fig.6. (a), (b), (c), (d), (e), and (f) are 0.73, 0.70, 0.43, 0.56, 0.36, 0.23, respectively. William et al. reported that human eye MTF drops to 0.40 at 10 Cyc/degree [17]. From our test lens, a drop in MTF value is observed at the outer area of the lens. At the zone boundaries of the outer zones, there is an expected chromatic effect; but the width of the phase distortion at zone boundaries are larger percentages of the zones, which is also lowering MTF. Further investigation to understand the contribution of the zone boundaries close to edges is important to know. For this purpose, we plan to do FDTD simulation at zone boundary areas for on-axis and off-axis light propagation. However, as it is expected the user will move his head to generally maintain a gaze angle less that about 25 degrees, the degradation of the MTF at larger angles may not be objectionable.

6. Conclusion

In this paper, we have shown a 5 cm aperture sized focus tunable liquid crystal lens. Pairing with an eye-tracking system, this proposed device holds a potential solution to solve well-known accommodation-convergence mismatch issue of HMDs. Due to its large aperture diameter and compact size, and fast switching speed, such a device can be used in ophthalmic or imaging applications.

7. Reference

[1] Mon-Williams M, Warm JP, Rushton S (1993) Binocular vision in a virtual world: visual deficits following the wearing of a head-mounted display. Ophthalmic and Physiological Optics 13:387–391

[2] Shibata T, Kawai T, Ohta K, Otsuki M, Miyake N, Yoshihara Y, Iwasaki T (2005) Stereoscopic 3-D display with optical correction for the reduction of the discrepancy between

accommodation and convergence. Journal of the Society for Information Display 13:665

[3] Lanman D, Luebke D (2013) Near-eye light field displays. ACM Transactions on Graphics 32:1–10

[4] Kwon Y-M (2011) Analysis of a head-mounted display-type multifocus display system using a laser scanning method. Optical Engineering 50:034006

[5] Love GD, Hoffman DM, Hands PJW, Gao J, Kirby AK, Banks MS (2009) High-speed switchable lens enables the development of a volumetric stereoscopic display. Optics Express 17:15716

[6] Maimone A, Georgiou A, Kollin JS (2017) Holographic near-eye displays for virtual and augmented reality. In: ACM Transactions on Graphics. Association for Computing Machinery, pp 1–16

[7] Development of a natural 3D display. https://spie.org/news/0659-development-of-a-natural-3d-display?SSO=1. Accessed 23 Nov 2020

[8] Kramida G (2016) Resolving the vergence-accommodation conflict in head-mounted displays. IEEE Transactions on Visualization and Computer Graphics 22:1912–1931

[9] Jamali A, Bryant D, Zhang Y, Grunnet-Jepsen A, Bhowmik A, Bos P (2017) 72-3: Design Investigation of Tunable Liquid Crystal Lens for Virtual Reality Displays. SID Symposium Digest of Technical Papers 48:1057–1060

[10] Jamali A, Bryant D, Zhang Y, Grunnet-Jepsen A, Bhowmik A, Bos P (2017) 72-3: Design Investigation of Tunable Liquid Crystal Lens for Virtual Reality Displays. SID Symposium Digest of Technical Papers 48:1057–1060

[11] Jamali A, Yousefzadeh C, McGinty C, Bryant D, Bos P (2018) LC lens systems to solve accommodation/convergence conflict in three-dimensional and virtual reality displays. Optical Engineering 57:1

[12] Stevens R, Jacoby TN, Aricescu IS, Rhodes DP (2017) A review of adjustable lenses for head mounted displays. 25

[13] Jamali A, Bryant D, Zhang Y, Grunnet-Jepsen A, Bhowmik A, Bos PJ (2018) Design of a large aperture tunable refractive Fresnel liquid crystal lens. Applied Optics 57:B10

[14] Jamali A, Bryant D, Bhowmick AK, Bos PJ (2020) Large area liquid crystal lenses for correction of presbyopia. https://doi.org/10.1364/OE.408770

[15] Li L, Bryant D, Bos PJ (2014) Liquid crystal lens with concentric electrodes and inter-electrode resistors. Liquid Crystals Reviews 2:130–154

[16] Li L, Bryant D, van Heugten T, Bos PJ (2013) Near-diffraction-limited and low-haze electro-optical tunable liquid crystal lens with floating electrodes. Optics Express 21:8371

[17] Watson, A. B. (2013). A formula for the mean human optical modulation transfer function as a function of pupil size. Journal of Vision, 13(6), 18